hydrology

MDPI

Article

Beyond One-Dimension: How Transient Groundwater Flow Amplifies Groundwater Evapotranspiration and Extinction Depth

Jia-Xin Shi [1,2], Linpeng Chen [3], Zhi-Yuan Zhang [2,4,*], Peng-Fei Han [2,4,*], Hongjuan Dong [5] and Zhenbin Zhang [1]

[1] School of Chemical and Environmental Engineering, Liaoning University of Technology, Jinzhou 121001, China; hgsjx@lnut.edu.cn (J.-X.S.)
[2] Key Laboratory of Groundwater Conservation of Ministry of Water Resources, China University of Geosciences, Beijing 100083, China
[3] State Environmental Protection Key Laboratory of Simulation and Control of Groundwater Pollution, Chinese Research Academy of Environmental Sciences, Beijing 100012, China
[4] Ministry of Education Key Laboratory of Groundwater Circulation and Environmental Evolution, China University of Geosciences, Beijing 100083, China
[5] School of Mining and Coal, Inner Mongolia University of Science and Technology, Baotou 014010, China
* Correspondence: zhiyuan.zhang@cugb.edu.cn (Z.-Y.Z.); pfhan@cugb.edu.cn (P.-F.H.)

Abstract

Accurate quantification of groundwater evapotranspiration (ET_g) is essential for reliable water resource assessment. Existing methods for estimating ET_g from water table fluctuation largely rely on one-dimensional simplifications that neglect transient groundwater flow. However, in areas with shallow water table and topographic relief, where transient groundwater flow often occurs, the validity and accuracy of this simplification remain inadequately evaluated. In this study, we used HYDRUS-2D to construct a 50 m-long sandy hillslope with a 0.05 gradient to investigate ET_g based on the water table fluctuation (WTF) method under transient groundwater flow conditions. The results indicate that periodic evapotranspiration generates water table fluctuations along the hillslope that exhibit amplitude attenuation and temporal phase lag, features not captured by 1D models. Ignoring transient groundwater flow leads to a systematic underestimation of ET_g by up to 85% in sandy soil near the topographic lows. Furthermore, we found that both the decoupling depth and the extinction depth are significantly amplified by lateral groundwater flow, by up to 66% and 51%, respectively, compared with 1D estimates derived from the Shah method. These findings highlight the importance of incorporating transient flow processes into ET_g estimation to improve the accuracy of water balance assessments and ecohydrological predictions, particularly in areas with shallow water tables and topographic relief.

Keywords: groundwater evapotranspiration; white method; extinction depth; transient groundwater flow; hillslope

Check for updates

Academic Editor: Peiyue Li

Received: 4 February 2026
Revised: 5 March 2026
Accepted: 12 March 2026
Published: 16 March 2026

Copyright: © 2026 by the authors. Licensee MDPI, Basel, Switzerland. This article is an open access article distributed under the terms and conditions of the Creative Commons Attribution (CC BY) license.

1. Introduction

Groundwater evapotranspiration (ET_g) represents a key linkage among the water, energy, and carbon cycles and constitutes a fundamental component of the water balance [1–3]. As one of the important sinks of groundwater [4], ET_g plays a critical role in water budgets and ecohydrological processes [5]. ET_g is controlled by complex factors, including atmospheric conditions, the hydrogeological environment, soil hydraulic properties, and water table depth [6].

Among these factors, water table depth is a primary driver of ET_g dynamics, with extensive literature confirming an inverse relationship between ET_g and water table depth [7–9]. At the regional scale, groundwater discharge to the atmosphere is often concentrated in topographic lows, such as riparian and lake shores, where the water table is shallow [10–12]. Consequently, the accurate quantification of ET_g is essential for groundwater management and ecological conservation in areas with a shallow water table.

In areas with a shallow water table, groundwater levels typically exhibits pronounced diurnal fluctuations driven by evapotranspiration, peaking in the early morning and reaching a minimum in the evening. Capitalizing on this phenomenon, White (1932) pioneered a method to estimate ET_g, laying the theoretical foundation for what are now known as water table fluctuation (WTF)methods [13]. Hays (2003) improved the calculation of White method by determining the net inflow rate based on water level changes between two consecutive days [14]. After that, Engel et al. (2005) improved White method by introducing an additive constant that represents the regional groundwater level change [15]. Subsequently, Loheide et al. (2008) and Gribovszki et al. (2008) further enhanced White method, enabling the precise estimation of net inflow rate on an hourly scale [16,17]. These approaches have been extensively applied across diverse climatic regimes [9,18], vegetation types [19,20], and groundwater depths [21,22], with further adaptation incorporating solar timing dynamics and soil water redistribution processes [23,24]. These methods enhance the accuracy of ET_g calculations. However, recent work by Su (2022) indicated that those improved methods do not improve ET_g estimation, and in some cases perform no better than the original White method [25]. This discrepancy suggests that the dominant source of uncertainty may not stem from the algorithmic modifications [26], but rather from an incomplete understanding of the mechanisms governing water table fluctuations under evapotranspiration forcing..

In areas characterized by shallow water table and topographic relief (e.g., riparian zones and lake shores), the magnitude of daily water table fluctuations typically diminishes with increasing distance from the surface water body. Concurrently, the timing of peak and trough water levels becomes progressively delayed along the hillslope [27,28]. These spatiotemporal patterns indicate that water table fluctuations are driven by not only in situ evapotranspiration but also significantly influenced by lateral groundwater flow [29]. Moreover, areas exhibiting strong diurnal water table fluctuations are often associated with upward hydraulic gradients [13,30,31], a critical factor that is frequently neglected in ET_g estimation. Consequently, the applicability and accuracy of WTF methods in environments dominated by lateral groundwater flow (from the surrounding environment) and deep groundwater recharge (from the underlying aquifers) remain inadequately explored.

In groundwater modeling, ET_g is typically calculated as a function of water table depth [32], and the approach proposed by Shah et al. [33] has been widely adopted to determine extinction depth and decoupling depth. However, this method involves rapid water table drawdown, forcing soil water content beyond equilibrium conditions (a stable state where net water movement ceases). This contrasts with field scenes, where water tables fluctuate within limited ranges and soil water content generally remains below equilibrium conditions [34,35]. Consequently, this approach may lead to an underestimation of ET_g [36]. Furthermore, in areas characterized by shallow water table and topographic relief, evapotranspiration can induce transient groundwater flow systems dominated by lateral flow [37,38]. These processes are neglected in one-dimensional models, suggesting that the relationship between ET_g and water table depth should be re-evaluated under transient groundwater flow conditions.

To address these questions, this study establishes a generalized two-dimensional lake–hillslope model that explicitly incorporates sloping topography, surface water boundaries,

deep groundwater recharge from a regional scale, and diurnally varying evapotranspiration. By systematically analyzing diurnal groundwater dynamics, groundwater flow systems evolution, and ET_g under transient flow conditions, this work aims to (1) show the phenomenon of groundwater fluctuation attenuation and lag along the hillslope under driven of evapotranspiration, (2) evaluate the bias of WTF methods on hillslopes, and (3) reveal the impact of transient groundwater flow systems on the relationship between ET_g and water table depth, and associated extinction depth and decoupling depth.

2. Materials and Methods

2.1. Methods for Estimating ET_g

2.1.1. WTF Methods

White (1932) first proposed quantifying ET_g using daily water table fluctuations [13] (Figure 1). The equation is as follows:

$$ET_g = S_y(24r \pm s), \tag{1}$$

where ET_g is the groundwater evapotranspiration over a 24 h period (L/T), r is the net inflow rate (L/T), s is the water storage over one day (L/T), and S_y is the specific yield (-). In areas with a shallow water table, the expression is as follows [39]:

$$S_y = \theta_s - \left[\theta_r + \frac{\theta_s - \theta_r}{\left[1 + (\alpha|d|)^n\right]^m}\right], \tag{2}$$

where d is depth to water table (L), θ_s is the saturated soil water content (-), θ_r is the residual soil water (-), α and n are soil parameters (-).

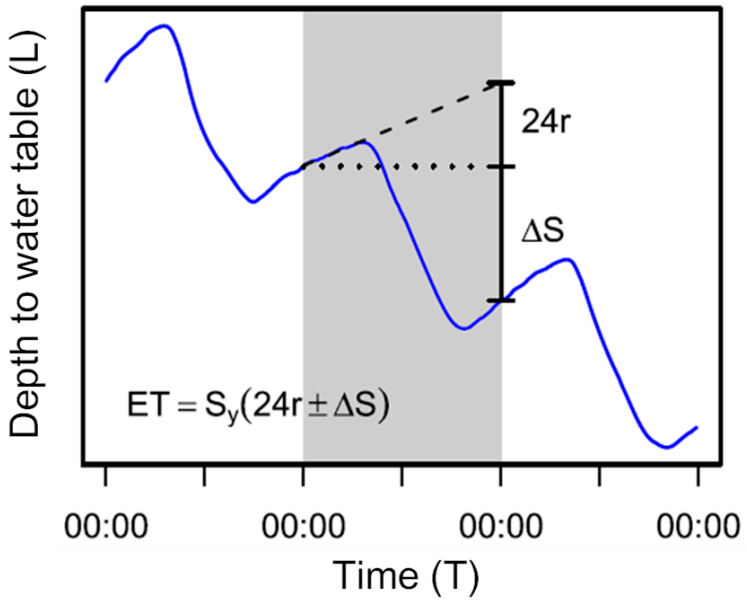

Figure 1. Illustration of the White method for estimation of ET_g based on water table fluctuation, the blue line is the groundwater level, and the day under investigation is highlighted in gray. (based on Fahle et al. [1]).

Loheide (2005) summarized the major assumptions of the White method [16], and proposed a new method to estimate the net inflow rate that varies over a 24 h period. The corresponding expression is given as follows:

$$S_y \frac{dWT}{dt} = r(t) - ET_g(t), \tag{3}$$

$\frac{dWT}{dt}$ is the water table change rate (L/T), S_y is the specific yield (-), $r(t)$ is the net inflow rate, which varies with time, and $ET_g(t)$ is the groundwater evapotranspiration, which also changes over time. Assuming that the water table of the recharge source remains constant, the net inflow rate is considered to be solely a function of water table depth. When nighttime ET_g equals zero, and Equation (3) becomes $r(WT) = S_y \frac{dWT}{dt}$, allowing the nighttime net inflow rate to be calculated. The daytime net inflow rate is then determined by fitting the relationship between water table and net inflow rate derived from two consecutive nights. Based on this relationship, $ET_g(t)$ can be estimated.

2.1.2. Water Balance Method

Shah (2007) estimated ET_g using a water balance method in HYDRUS-1D [33]. When the entire soil profile is driven solely by evapotranspiration, and there is no external water input, the total water loss from the system is assumed to be equal to evapotranspiration (ET). Under these conditions, ET can be calculated as follows:

$$ETL|t_i = \int_{\Delta S} \theta_{model} dz|t_{i-1} - \int_{\Delta S} \theta_{model} dz|t_i, \quad (4)$$

where ETL is the total evapotranspiration loss during a given time step (L); θ_{model} is the simulated water content (-), with i representing the time index (T); and ΔS is the length of the soil column [L]. The ET rate can then be calculated as follows:

$$ET = \frac{ETL}{\Delta t}, \quad (5)$$

where $\Delta t = t_i - t_{i-1}$ is the time step (T). ET_g is assumed to be supplied solely by groundwater, without any contribution from the vadose zone (VZC). Based on the principle of mass balance, total evapotranspiration can be partitioned into vadose zone evapotranspiration and ET_g. Accordingly, ET_g can be expressed as follows:

$$ET_g = ET - ET_s, \quad (6)$$

where ET is the total evapotranspiration (L/T), ET_s is soil water evapotranspiration (L/T). Mathematically, ET_s can be calculated using the trapezoidal rule of integration based on the simulated water content within the vadose zone.

2.2. Numerical Model

2.2.1. Governing Water Flow Equations

The HYDRUS-2D (Version 2.04) model uses the Richards equation to simulate variable saturated water flow processes [40]. It has been widely used to simulate evapotranspiration (ET) and water table fluctuations [23]. The governing equation for the HYDRUS-2D model is as follows:

$$\frac{\partial \theta}{\partial t} = \nabla \cdot (K\nabla h + K\nabla z) - S, \quad (7)$$

where θ represents soil water content (-), t denotes time (T), $\bigtriangledown$ is the velocity tensor operator (1/L), K is the unsaturated hydraulic conductivity (L/T), which is related to saturation, h is the pressure head (L), z is the gravitational head (L), and S represents the sink term for root water uptake (1/T). The root water uptake calculation method is based on the Feddes function [41], and the formula is as follows:

$$S(h) = \alpha(h)B(z)T_p, \quad (8)$$

where α(h) is a prescribed dimensionless function, which is related to soil suction h(-), B(z) is the normalized root water uptake distribution function (1/L), which can be obtained by normalizing any measured root distribution data or a specified root distribution function, and T_p is the potential transpiration rate (L/T), and can be calculated from meteorological data to obtain potential evapotranspiration, which is then used with Beer's formula [42]. The formula is as follows:

$$T_P = ET_P(1 - e^{-k*LAI}) = ET_P SCF, \quad (9)$$

$$E_P = ET_P e^{-k*LAI} = ET_P(1 - SCF), \quad (10)$$

where ET_p denotes potential evapotranspiration (L/T), E_p is potential evaporation (L/T), and LAI is the leaf area index (-). The LAI is set to 0.24, according to the studies in arid and semi-arid areas [43,44]. The parameter k is a constant governing the radiation extinction by the canopy (-), with a value of 0.48, and SCF represents soil cover fraction (-), which is calculated as a function of LAI. The root depth was set to 15 cm to represent *Carex duriuscula* in arid and semiarid areas [45]. The root density decreases linearly and is uniformly distributed across the profile.

2.2.2. Model Construction

A generalized two-dimensional lake–hillslope was constructed based on the concept of hydrologic landscapes [46] (Figure 2). The hillslope extends 50 m in the horizontal direction, with a vertical depth of 10 m and a slope of 0.05 (the ratio of the opposite side to the adjacent side). The shoreline length was set to 5 m. According to the previous studies of the lake shore, the soil texture in the lake bottom is usually finer, and the hydraulic conductivity of sediments near the lake bottom is substantially lower than that of the rest of the 2D domain [43,47]. Therefore, the soil composition of the entire hillslope is divided into two zones. For the lake-bottom zone (5 m in length from the lakeshore and 1 m in depth), the hydraulic conductivity was reduced while maintaining other soil hydraulic parameters unchanged. This approach represents the low permeability conditions of the lake bottom while minimizing the influence of soil heterogeneity. The remaining soil type of the 2D domain is set to sand (changing into loam and silt in Section 3.4). The soil types for the rest of the 2D domain are selected from the HYDRUS database, with the soil hydraulic parameters detailed in Table 1.

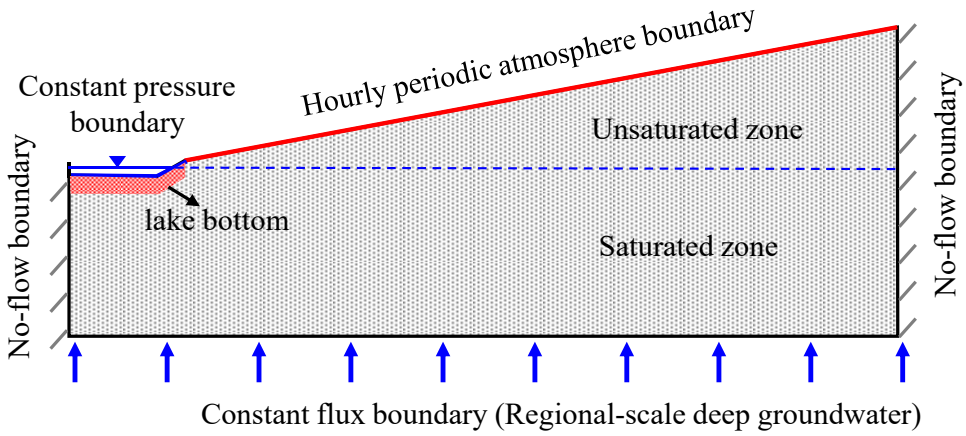

Figure 2. The conceptual two-dimensional hillslope.

Table 1. Soil Hydraulic Parameters.

Zone		θ_s (cm^3/cm^3)	θ_r (cm^3/cm^3)	α (cm^{-1})	n (-)	K_s (cm/d)
The rest of the 2D domain	Sand	0.43	0.045	0.145	2.68	713
	Loam	0.43	0.078	0.036	1.56	24.96
	Silt	0.46	0.034	0.016	1.37	6
Lake bottom zone		Same as the rest of the 2D domain	Same as the rest of the 2D domain	Same as the rest of the 2D domain	Same as the rest of the 2D domain	10

The finite element mesh length is uniformly set to 40 cm, which is refined to 15 cm at the model surface. The final mesh consists of 11,212 nodes and 22,040 finite elements. The lake water level is set to be constant to represent a stable surface water supply. To characterize the upward discharge from deep groundwater, the bottom boundary is specified as a constant flux boundary with a discharge rate of 1 mm/d based on former studies in groundwater discharge areas [36,43,48,49]. The left and right sides of the model correspond to the lake center and topographic divide, respectively, assuming no water exchange and set as no flux boundaries according to former research [50–52]. The remainder of the upper boundary is set as an atmosphere boundary to account for the effects of cyclical evapotranspiration on the hillslope. As described in Equation (11). The periodic variation in potential evapotranspiration is expressed using a piecewise sine function. The formula is as follows:

$$ET_p = \begin{cases} 0 & t < 6, t > 18 \\ 1.58 \sin\left(\frac{2\pi t}{24} - \frac{\pi}{2}\right) & 6 \le t \le 18 \end{cases}, \quad (11)$$

where t is time (T), ET_p represents potential evapotranspiration (L/T), and the cumulative evapotranspiration within a day amounts to 12.0 mm/d, which is based on potential evapotranspiration (PET) representative of arid and semi-arid regions [23,33,53], with a periodic cycle of 24 h.

The initial condition of the model is set with a pressure head of 990 cm at the model bottom, which is uniformly distributed throughout the domain under the assumption of hydrostatic equilibrium. A warm-up simulation period of 2400 h is conducted to allow the soil–groundwater system to reach a stable, periodically fluctuating state, in which soil water content and water table variations within each cycle repeat the dynamics of the preceding cycle. Groundwater flow fields obtained after 2400 h are selected for analysis. During the simulations, the minimum and maximum time steps are set to 0.0024 h and 1 h, respectively. The relative error in water balance calculations is maintained below 5%, ensuring the accuracy and reliability of the model results.

3. Results

3.1. Transient Evolution of Groundwater Depression Under Periodic Evapotranspiration

As shown in Figure 3, the groundwater depression exhibits periodic emergence and disappearance at the daily scale in response to evapotranspiration forcing. The water table along the hillslope reaches its maximum at approximately 07:00, when the groundwater depression is least developed, and the hydraulic gradient from the topographic highs to the lows is minimal (approximately 0.00025). As evapotranspiration progresses, the groundwater depression gradually deepens. At 17:00, the groundwater depression becomes most pronounced, the hydraulic gradient from topographic highs to lows increases to its maximum value of approximately 0.00053, and the water table across the hillslope reaches its minimum. During the evening and nighttime, as evapotranspiration ceases, groundwater depression is progressively replenished by lateral groundwater flow and

deep groundwater discharge, resulting in gradual recovery of the water table depression. The water table subsequently rises and reaches its maximum again at 7:00 of the following day, completing a full diurnal cycle.

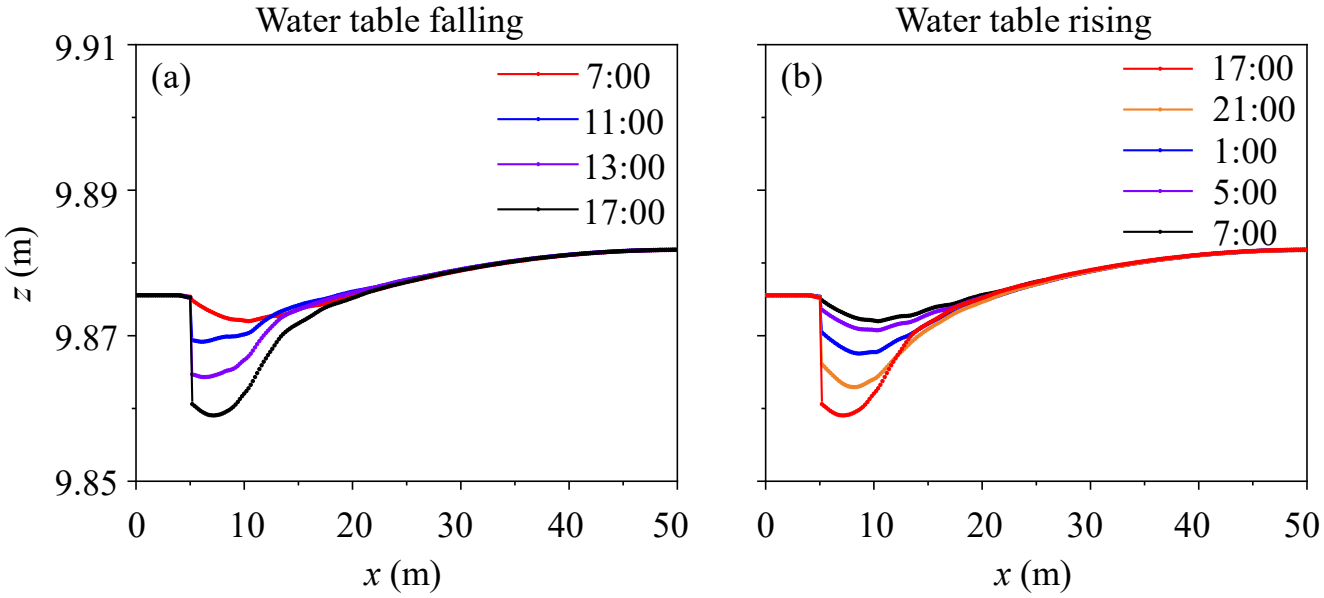

Figure 3. The groundwater fluctuations at the hourly scale: (**a**) the formation of groundwater depression; (**b**) the recovery of groundwater depression.

3.2. Spatial Attenuation and Phase Lag of Water Table Fluctuations in the Hillslope

Analysis of groundwater fluctuation characteristics (Figure 4) shows that the daily water table fluctuation amplitude decreases along the *x-axis* (Figure 4a). The maximum daily fluctuation amplitude occurs near the water table at topographic lows, exceeding 1.4 cm, whereas the minimum daily fluctuation amplitude is observed near the water table at the topographic highs (x = 50 m), where it is less than 0.1 cm. At topographic lows, for a fixed x position, the daily groundwater fluctuation amplitude also decreases with increasing depth along the z-axis. For example, compared with the maximum fluctuation amplitude exceeding 1.4 cm near z = 10 m, it decreases to less than 0.8 cm near z = 5 m.

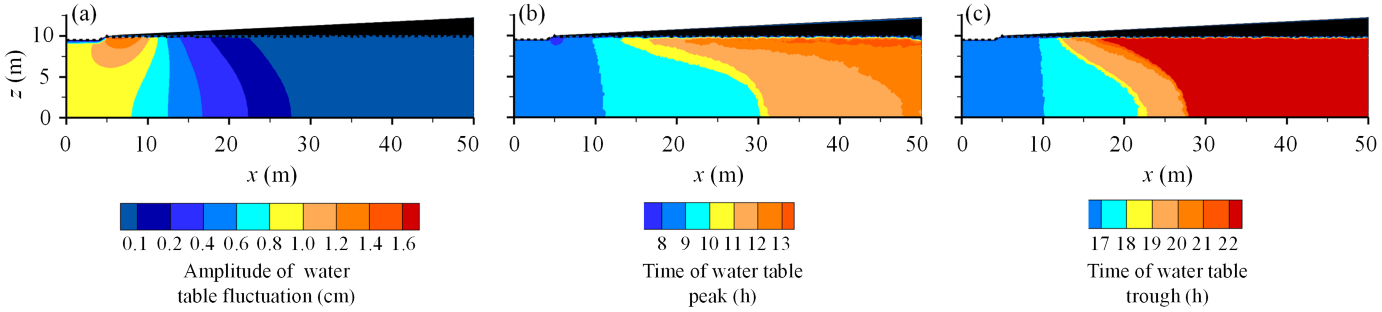

Figure 4. The distribution of groundwater fluctuation amplitude and response time: (**a**) fluctuation amplitude; (**b**) the time of peak of water table; (**c**) the time of trough of water table.

As shown in Figure 4b, the time of the water table peak shifts progressively to later times along the x-axis. At topographic lows, the water table peak coincides with the onset of evapotranspiration at approximately 07:00, whereas at the topographic highs the peak occurs much later, approaching 12:00. A similar spatial pattern is observed for water table trough time (Figure 4c). Specifically, the earliest water table trough occurs at the

topographic lows at approximately 17:00, while the latest water table trough occurs at the topographic highs at around 21:00.

The combined patterns of fluctuation amplitude, peak time, and trough time indicate that under evapotranspiration forcing, groundwater dynamics across the hillslope are primarily controlled by groundwater fluctuations at the topographic lows. Groundwater fluctuations in other parts of the hillslope are mainly controlled by the propagation of hydraulic fluctuations originating from the topographic lows.

3.3. Effects of Water Table Propagation on WTF Methods

To evaluate the accuracy of ET_g estimates derived from the WTF methods in hourly scale, ten right-angled trapezoidal units are selected to analyze ET_g and groundwater inflow. Each unit was 1 m wide, and its center points were distributed along the hillslope at distances ranging from 6 to 22 m (Figures 4 and 5). Daily groundwater dynamics for these ten units were extracted from the numerical simulations. Based on the daily water table fluctuation patterns, ET_g for each unit is calculated using both the White method and the Loheide method [13,16]. The ET_g directly obtained from the numerical model is taken as the actual ET_g [23], and is hereafter referred to as the model-simulated ET_g. The values calculated using the different WTF methods are denoted as the White-method and Loheide-method estimates, respectively (Figure 5).

As shown in Figure 5, discrepancies exist between the ET_g values estimated by the White method, Loheide method, and the model-simulated values, with the estimated ET_g exhibiting increasingly pronounced time lag characteristics as distance along the *x-axis* increases. With increasing distance along the *x-axis*, the WTF methods initially underestimate and subsequently overestimate the actual ET_g. When x is less than 10 m, both the White and Loheide methods systematically underestimate ET_g. In contrast, when x is greater than 10 m, both methods significantly overestimate ET_g.

This transition in estimation values is related to the spatial evolution of groundwater flow conditions. At smaller x values, the water table is shallow, and a groundwater depression develops. In this location, groundwater is replenished by lateral groundwater flow from lake water and topographic highs. These recharge sources mitigate the decline in water table induced by evapotranspiration, leading to underestimation by WTF methods. As x increases beyond the groundwater depression, groundwater recharge decreases. In these areas, water table fluctuations are not solely driven by in situ evapotranspiration but are also influenced by laterally propagated hydraulic fluctuations originating from the topographic low. This superposition introduces additional time-lagged fluctuations, resulting in an overestimation of ET_g when the WTF methods are applied.

The model-simulated ET_g and the WTF estimated ET_g show no significant lag when x is less than 9 m. However, a pronounced lag emerges when x exceeds 9 m and becomes particularly evident at x = 11 m. At this site, a clear discrepancy between model-simulated and estimated ET_g values indicates that the WTF methods are no longer applicable. The water table fluctuations at this site are dominated by the lateral transmission of hydraulic signals from the topographic lows rather than by in situ evapotranspiration.

In summary, comparison of hourly ET_g rates at different sites along the hillslope demonstrates that the applicability of WTF methods is limited. When water table fluctuations are influenced by transient lateral groundwater flow, applying the WTF methods to estimate ET_g can introduce substantial errors.

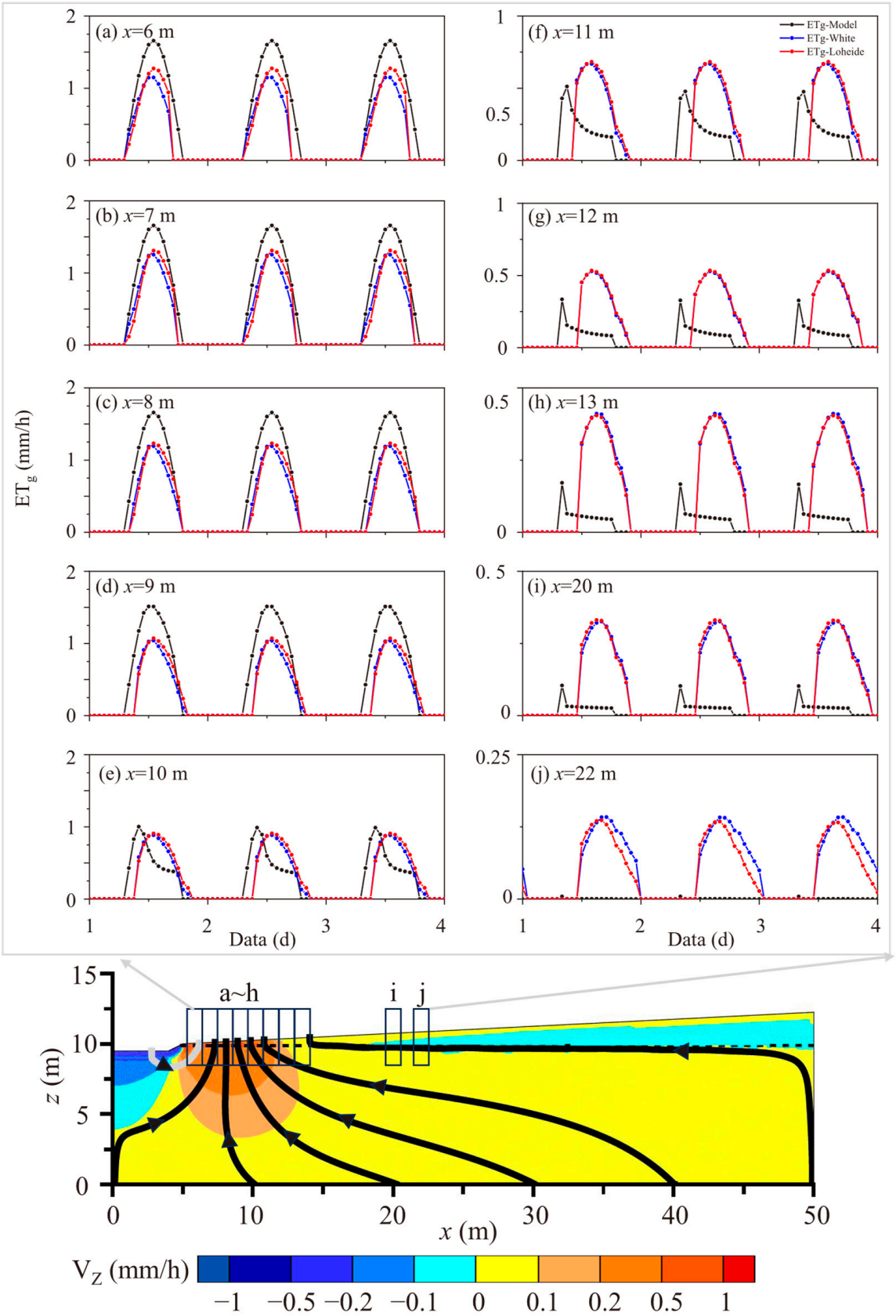

Figure 5. Simulated ET_g values and calculated variations for selected units in hourly scale: (**a**–**h**) represent units at x = 6 to 13 m; (**i**) and (**j**) correspond to units at x = 20 m and x = 22 m, respectively.

3.4. Accuracy of ET_g Calculations Using Different WTF Methods

Water table fluctuations affect the accuracy of ET_g estimates. To evaluate the performance of WTF methods, daily ET_g values derived from two approaches are compared with the actual ET_g, which was obtained from the numerical model (Figure 6, Table 2). As shown in Figure 4, when x exceeds 14 m, the amplitude of water table fluctuations decreases markedly, and the actual ET_g approaches zero. Therefore, the comparison between calculated and simulated daily ET_g values is restricted to the lakeshore where $x < 14$ m. To further examine the influence of soil properties on ET_g estimation accuracy, the soil type was systematically changed from sand to loam and silt while keeping the lake-bottom soil properties unchanged. The accuracy of White method and the Loheide method under different soil conditions was then evaluated.

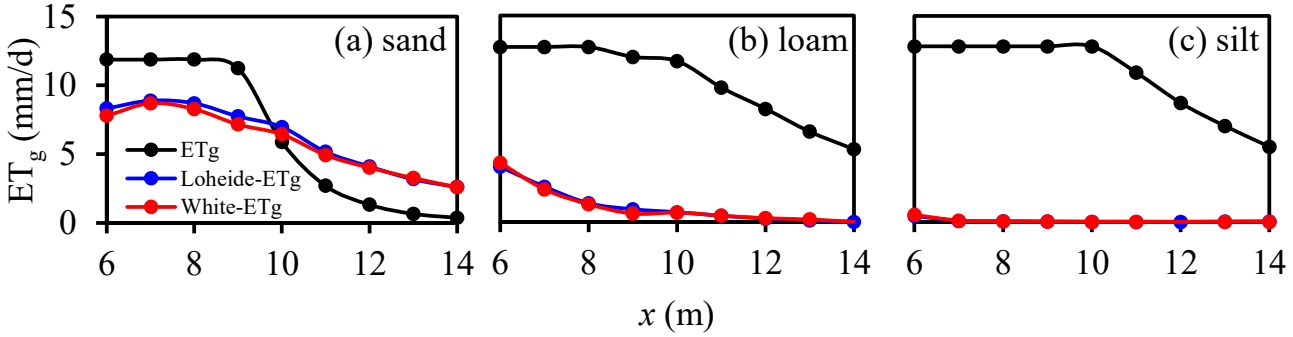

Figure 6. Comparison of actual and simulated ET_g values for different soil types.

Table 2. Comparative performance of the Loheide and White methods.

Soil Type	**Sand**		**Loam**		**Silt**	
Method	Loheide	White	Loheide	White	Loheide	White
R^2	0.9387	0.9353	0.5017	0.4278	0.0942	0.1341
Bias	−0.240	−0.519	−8.435	−8.449	−9.873	−9.866
RMSE	2.796	2.999	8.643	8.673	10.187	10.177
MEA	2.7025	2.8108	8.4349	8.4491	9.873	9.8662

As shown in Figure 6, under sloping topography, none of the methods can accurately estimate ET_g in the three soil types. For sandy soils (Figure 6a), ET_g is underestimated at the topographic lows where the water table is shallow, with both the White and Loheide methods exhibiting a maximum underestimation of 1.57 times. However, as the x increases and the water table deepens, the estimation shifts from underestimation to overestimation when x exceeds 10 m. The magnitude of overestimation further increases with distance along the x-axis, reaching a maximum of 7.06 times for both methods. Table 2 indicates that although both the Loheide and White methods exhibited relatively low Bias and MAE, a certain degree of underestimation still exists in this scenario.

For loam soils (Figure 6b), ET_g is consistently underestimated across the entire hillslope, with an underestimation degree ranging from 2.95 to 64 times. The lower hydraulic conductivity of loam restricts water table fluctuations, leading to attenuated water table variations. Under these conditions, the White method and Loheide method consistently reflect underestimation. For silt soils (Figure 6c), the hydraulic conductivity is further reduced, resulting in a narrower spatial extent of daily groundwater fluctuations. As a consequence, the WTF methods exhibit a pronounced underestimation. Consequently, as shown in Table 2, both methods exhibit pronounced underestimation, with Bias approaching −9.87 and RMSE exceeding 10.

In summary, under sloping topography, water table fluctuations are influenced by the transient lateral groundwater flow, making the WTF methods incapable of accurately calculating ET_g. Even in zones where there is no pronounced time lag in water table fluctuations, ET_g remains underestimated for all three soil types.

4. Discussion

4.1. Evolution of Daily Scale Periodic Groundwater Flow Systems

The groundwater flow field exhibits pronounced transient characteristics under hourly-scale periodic evapotranspiration forcing (Figure 7). Under evapotranspiration forcing, there will be three groundwater flow systems in the hillslope: one from the lake to the aquifer, one from the model bottom to the surface, and one from topographic highs to topographic lows. These groundwater flow systems evolve rapidly over time, reflecting strong transient dynamics.

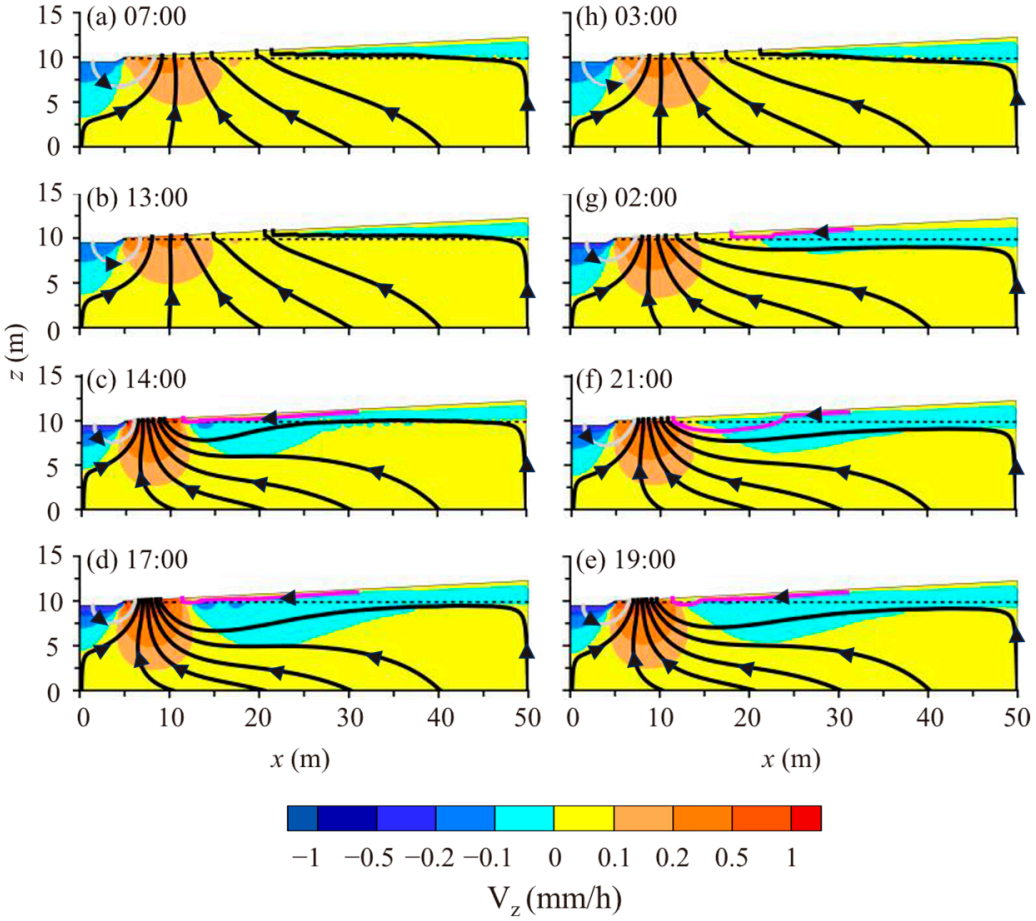

Figure 7. The evolution of the groundwater flow system occurs hourly: (**a**–**h**) represent the hours from 7 a.m. to 3 a.m. of the next day; arrows indicate the direction of the water flow, streamlines in different colors denote different groundwater flow systems.

At 7:00, the local flow system from topographic highs to topographic lows has not yet developed, while the range of deep groundwater from the model bottom to the surface exhibits a larger extent (Figure 7a). As evapotranspiration progresses and groundwater depression expands, a local flow system from the topographic highs to topographic lows begins to emerge at approximately 14:00, converging groundwater from the model bottom towards topographic lows. At 17:00, this local flow system reaches its maximum development, extending laterally from x = 12 m to x = 50 m. The maximum penetration depth

of this local flow system also peaked at this time, reaching approximately 4.9 m below the water table (Figure 7d). Consequently, groundwater from the model bottom becomes increasingly concentrated at topographic lows.

During the evening and nighttime, as the groundwater depression gradually recovers, the local flow system weakens, and its extent diminishes. At 02:00, the local flow system has largely dissipated (Figure 7g). At this time, groundwater recharge across the hillslope becomes relatively uniform and reaches its maximum extent. This condition contrasts sharply with that at 17:00, when groundwater recharge is strongly focused toward topographic lows. Overall, the hillslope topography induces spatially heterogeneous evapotranspiration, which drives the formation and dissipation of groundwater depressions and leads to the cyclic emergence and disappearance of local flow systems.

4.2. Spatiotemporal Variability of Groundwater Recharge Sources

To investigate the groundwater sources contributing to ET_g (Figure 8), groundwater recharge pathways are identified using the streamline tracing method. The boundaries of deep groundwater recharge are delineated by the blue and red lines, respectively. Areas located to the left of the blue line are recharged by lake water, whereas areas to the right of the red line receive no groundwater recharge. The region between the two boundaries is supplied by deep groundwater from the model bottom.

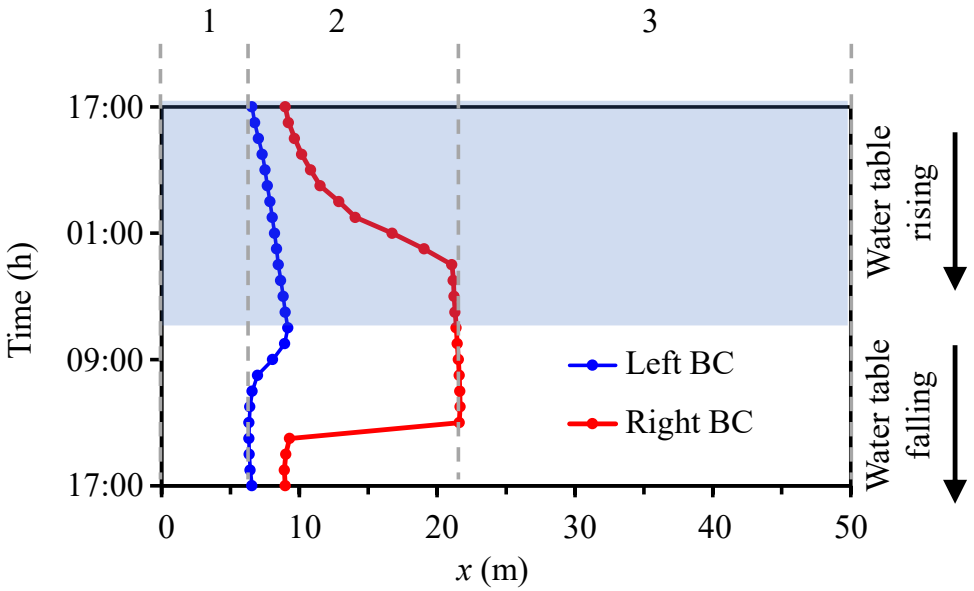

Figure 8. The spatiotemporal variability of groundwater recharge sources from the model bottom.

As shown in Figure 8, the depth to the base of the deep groundwater layer varies significantly over a single diurnal cycle, and locations along the x-axis experience different degrees of recharge. At 17:00, when the water table reaches its minimum and the groundwater depression is most pronounced, the local flow system is most developed. Under these conditions, deep groundwater to the surface is restricted to a narrow range of only 2.53 m, extending from x = 6.54 to x = 9.07 m. Following the cessation of evapotranspiration, the groundwater depression gradually recovers. Consequently, both the left and right boundaries of the deep groundwater shift towards the positive x direction, resulting in an expansion of the deep groundwater area. At 07:00, when the groundwater depression is weakest, the left boundary shifts to x = 9.17 m, while the right boundary extends to x = 21.38 m.

Based on the spatial distribution of recharge sources, groundwater recharge along the *x-axis* can be classified into three zones from left to right: (1) lake water recharge zone,

within the range of 5 to 6.54 m; (2) deep groundwater recharge zone, within the range of 6.54 to 21.38 m; and (3) no groundwater recharge zone, with *x-axis* exceeding 21.6 m. Within the deep groundwater recharge zone, a sub-region between 6.54 and 9.17 m receives recharge from both lake water and deep groundwater.

These results demonstrate that groundwater recharge sources exhibit pronounced spatial heterogeneity, even over short distances. Moreover, the groundwater recharge sources at a given location are not static but vary dynamically in response to the development and decay of local flow systems.

4.3. Enhancement of Extinction Depths Under the Influence of Transient Groundwater Flow

According to the definition proposed by Shah [33], when the soil water content in the vadose zone remains unchanged, and the water table is stable, the water storage deficit within the vadose zone remains constant. Under such conditions, all evapotranspiration at a given location is supplied by groundwater. In our simulation, the entire two-dimensional hillslope reaches a periodically stable state within a certain range under cyclic evapotranspiration. Within each diurnal cycle, the water table returns to its initial position, and the soil water content throughout the vadose zone remains nearly unchanged, with daily variations of less than 1‰. Consequently, both water table and soil water distributions recover to their initial states at the end of each cycle. Therefore, water storage within the vertical soil column at any given position along the *x-axis* remains constant over one cycle. Under these periodically stable conditions, soil water evapotranspiration is zero, and ET_g equals the total evapotranspiration. Based on the principle of water balance, ET_g can therefore be quantified as the upward vertical flux across the water table. By extracting this vertical flux at different locations along the hillslope, ET_g values corresponding to different water table depths can be obtained, allowing the relationship between ET_g and water table depth to be determined. For the 1D model, a periodically varying evapotranspiration boundary at the hourly scale was applied at the upper boundary, consistent with the 2D model and described by Equation (11). The lower boundary was specified as a no-flux boundary. The soil type was standard sand, identical to that used in the 2D model. The model depth was 5 m and was discretized into 501 nodes. The initial condition assumed a fully saturated profile. Under the influence of evapotranspiration, the groundwater table gradually declined, allowing the relationship between groundwater evapotranspiration and groundwater table depth to be obtained. The subsequent estimation of ET_g was conducted in strict accordance with the methodology outlined by Shah [33].

Using this approach, ET_g at different water table depths under varying slope gradients is obtained and compared with one-dimensional simulation results using Shah's method (Figure 9). The results show that ET_g is significantly enhanced compared to one-dimensional conditions due to the influence of transient groundwater flow. This enhancement is most pronounced at a slope of 0.03 and least pronounced at 0.10. For example, at a water table depth of 30 cm, the ratio of ET_g to potential evapotranspiration reaches 1.00 for a slope of 0.03, whereas the corresponding value from the one-dimensional simulation is only 0.05. At this low slope, the deviation from the one-dimensional simulation results is greatest, indicating a strong enhancement of ET_g. In contrast, at a slope of 0.10, the relationship between ET_g and water table depth nearly coincides with the one-dimensional simulation results when the water table is shallower than 15.8 cm.

The decoupling depth of ET_g exhibits a decreasing trend with an increasing slope. For slopes of 0.03, 0.05, 0.07, 0.09, and 0.10, the decoupling depths are 39.8, 17.1, 15.2, 11.2, and 10.6 cm, respectively, whereas the one-dimensional simulation yields a constant value of only 10.6 cm. A similar trend is observed for the extinction depth of ET_g. As the slope

increases from 0.03 to 0.10, the extinction depths decrease from 81.5 to 49.1 cm, compared with only 40.1 cm in the one-dimensional simulation.

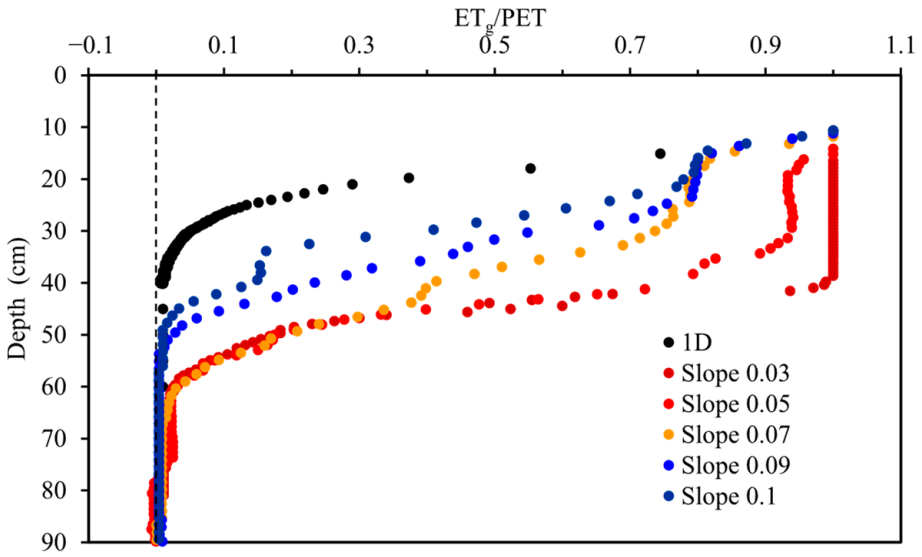

Figure 9. Comparison of ET_g vs. water table depth at different slopes.

These behaviors arise because an increasing slope narrows the evapotranspiration range, weakens groundwater depressions, and reduces recharge from multiple groundwater flow systems, causing ET_g closer to one-dimensional simulation results. These findings demonstrate that in areas with shallow water table and topographic relief, the emergence of transient groundwater flow significantly enhances ET_g. In contrast, the conventional methodologies that neglect the effects of groundwater flow and assume steady-state groundwater flow conditions tend to underestimate ET_g.

5. Conclusions

This study provides new mechanistic insight into how transient groundwater flow reshapes ET_g dynamics in areas with shallow water tables and topographic relief. By developing a two-dimensional variably saturated flow model using HYDRUS-2D, we demonstrate that uneven evapotranspiration induces cyclic groundwater depressions at topographic lows and activates dynamically evolving groundwater flow systems, generating diurnal water table fluctuations with amplitude attenuation and phase lag. The propagation of water table fluctuations leads to a systematic underestimation of ET_g. In a sandy hillslope scenario with a slope of 0.05, the White and Loheide methods underestimate ET_g near topographic lows, with maximum underestimation reaching 1.57 times. While in loam and silt soils, ET_g is consistently underestimated when the consistency of water table fluctuations is ignored, with the maximum underestimation reaching 64 times. Furthermore, comparisons of ET_g under different slope conditions and the 1D scenario demonstrate that transient groundwater flow substantially enhances ET_g. Specifically, in the sandy soil scenario, the decoupling depth increases by up to 20.4 cm and the extinction depth by up to 41.4 cm compared with 1D estimates derived from the Shah method.

These findings highlight the importance of transient groundwater flow in ET_g estimation. Despite its strengths, this research relies on idealized hillslope geometries and homogeneous soil profiles (sand, loam, and clay). In field conditions, soil heterogeneity may further complicate the propagation of diurnal water table signals. In addition, vegetation characteristics (e.g., root depth and LAI) were fixed and simplified, without considering seasonal dynamics. The model represents an idealized hillslope–lake system and lacks

field validation. Future work should focus on modifying the 1D model by incorporating groundwater lateral flow, and combining numerical modeling with high resolution groundwater and soil moisture monitoring to quantify transient flow contributions to ET_g under laboratory by a sloping soil lysimeter.

Overall, these findings advance ecohydrological understanding by identifying transient groundwater flow control on ET_g under sloping topography. The approach offers valuable insights for WTF methods in riparian zones, lake shores, and other areas with shallow water table and topographic relief, enhancing the accuracy of water balance assessment and groundwater management decisions.

Author Contributions: Conceptualization, J.-X.S. and Z.-Y.Z.; methodology, J.-X.S. and P.-F.H.; software, J.-X.S.; validation, L.C. and H.D.; writing—original draft preparation, J.-X.S.; writing—review and editing, J.-X.S. and Z.-Y.Z.; visualization, J.-X.S.; supervision, Z.Z. All authors have read and agreed to the published version of the manuscript.

Funding: This research was funded by the National Natural Science Foundation of China (42402251, 42302280), the Natural Science Foundation of Liaoning Province (2025-BS-0496), and the Key Laboratory of Groundwater Conservation of Ministry of Water Resources Foundation.

Data Availability Statement: Data used in the research is available from the corresponding author upon request.

Conflicts of Interest: The authors declare no conflicts of interest.

Abbreviations

The following abbreviations are used in this manuscript:

ET_g	groundwater evapotranspiration
WTF	Water table fluctuation

References

1. Fahle, M.; Dietrich, O. Estimation of evapotranspiration using diurnal groundwater level fluctuations: Comparison of different approaches with groundwater lysimeter data. *Water Resour. Res.* **2014**, *50*, 273–286. [CrossRef]
2. Jung, M.; Reichstein, M.; Ciais, P.; Seneviratne, S.I.; Sheffield, J.; Goulden, M.L.; Bonan, G.; Cescatti, A.; Chen, J.; de Jeu, R.; et al. Recent decline in the global land evapotranspiration trend due to limited moisture supply. *Nature* **2010**, *467*, 951–954. [CrossRef] [PubMed]
3. Senay, G.B.; Leake, S.; Nagler, P.L.; Artan, G.; Dickinson, J.; Cordova, J.T.; Glenn, E.P. Estimating basin scale evapotranspiration (ET) by water balance and remote sensing methods. *Hydrol. Process.* **2011**, *25*, 4037–4049. [CrossRef]
4. Nichols, W.D. Groundwater discharge by phreatophyte shrubs in the Great Basin as related to depth to groundwater. *Water Resour. Res.* **1994**, *30*, 3265–3274. [CrossRef]
5. Babajimopoulos, C.; Panoras, A.; Georgoussis, H.; Arampatzis, G.; Hatzigiannakis, E.; Papamichail, D. Contribution to irrigation from shallow water table under field conditions. *Agric. Water Manag.* **2007**, *92*, 205–210. [CrossRef]
6. Chen, L.; Wang, W.K.; Zhang, Z.Y.; Wang, Z.F.; Wang, Q.M.; Zhao, M.; Gong, C.C. Estimation of bare soil evaporation for different depths of water table in the wind-blown sand area of the Ordos Basin, China. *Hydrogeol. J.* **2018**, *26*, 1693–1704. [CrossRef]
7. Cooper, D.J.; Sanderson, J.S.; Stannard, D.I.; Groeneveld, D.P. Effects of long-term water table drawdown on evapotranspiration and vegetation in an arid region phreatophyte community. *J. Hydrol.* **2006**, *325*, 21–34. [CrossRef]
8. Fan, Y.; Miguez-Macho, G. Potential groundwater contribution to Amazon evapotranspiration. *Hydrol. Earth Syst. Sci.* **2010**, *14*, 2039–2056. [CrossRef]
9. Lautz, L.K. Estimating groundwater evapotranspiration rates using diurnal water-table fluctuations in a semi-arid riparian zone. *Hydrogeol. J.* **2007**, *16*, 483–497. [CrossRef]
10. Fan, Y.; Li, H.; Miguez-Macho, G. Global Patterns of Groundwater Table Depth. *Science* **2013**, *339*, 940–943. [CrossRef]
11. Maxwell, R.M.; Condon, L.E.; Danesh-Yazdi, M.; Bearup, L.A. Exploring source water mixing and transient residence time distributions of outflow and evapotranspiration with an integrated hydrologic model and Lagrangian particle tracking approach. *Ecohydrology* **2019**, *12*, E2042. [CrossRef]

12. Soylu, M.E.; Istanbulluoglu, E.; Lenters, J.D.; Wang, T. Quantifying the impact of groundwater depth on evapotranspiration in a semi-arid grassland region. *Hydrol. Earth Syst. Sci.* **2011**, *15*, 787–806. [CrossRef]
13. White, W.N. *A Method of Estimating Ground-Water Supplies Based on Discharge by Plants and Evaporation from Soil: Results of Investigations in Escalante Valley, Utah*; U.S. Government Printing Office: Washington, DC, USA, 1932; p. 105.
14. Hays, K.B. Water Use by Saltcedar (*Tamarix* sp.) and Associated Vegetation on the Canadian, Colrado and Pecos Rivers in Texas. Master's Thesis, Texas A&M University, College Station, TX, USA, 2003.
15. Engel, V.; Jobbágy, E.G.; Stieglitz, M.; Williams, M.; Jackson, R.B. Hydrological consequences of Eucalyptus afforestation in the Argentine Pampas. *Water Resour. Res.* **2005**, *41*, W10409. [CrossRef]
16. Loheide, S.P. A method for estimating subdaily evapotranspiration of shallow groundwater using diurnal water table fluctuations. *Ecohydrology* **2008**, *1*, 59–66. [CrossRef]
17. Gribovszki, Z.; Kalicz, P.; Szilágyi, J.; Kucsara, M. Riparian zone evapotranspiration estimation from diurnal groundwater level fluctuations. *J. Hydrol.* **2008**, *349*, 6–17. [CrossRef]
18. Ciruzzi, D.M.; Loheide, S.P., II. Groundwater subsidizes tree growth and transpiration in sandy humid forests. *Ecohydrology* **2021**, *14*, e2294. [CrossRef]
19. Diouf, O.C.; Weihermüller, L.; Diedhiou, M.; Vereecken, H.; Faye, S.C.; Faye, S.; Sylla, S.N. Modelling groundwater evapotranspiration in a shallow aquifer in a semi-arid environment. *J. Hydrol.* **2020**, *587*, 124967. [CrossRef]
20. Fan, J.; Oestergaard, K.T.; Guyot, A.; Lockington, D.A. Estimating groundwater recharge and evapotranspiration from water table fluctuations under three vegetation covers in a coastal sandy aquifer of subtropical Australia. *J. Hydrol.* **2014**, *519*, 1120–1129. [CrossRef]
21. Cheng, D.-H.; Li, Y.; Chen, X.; Wang, W.-K.; Hou, G.-C.; Wang, C.-L. Estimation of groundwater evaportranspiration using diurnal water table fluctuations in the Mu Us Desert, northern China. *J. Hydrol.* **2013**, *490*, 106–113. [CrossRef]
22. Yin, L.; Zhou, Y.; Huang, J.; Wenninger, J.; Zhang, E.; Hou, G.; Dong, J. Interaction between groundwater and trees in an arid site: Potential impacts of climate variation and groundwater abstraction on trees. *J. Hydrol.* **2015**, *528*, 435–448. [CrossRef]
23. Jia, W.; Yin, L.; Zhang, M.; Zhang, J.; Zhang, X.; Gu, X.; Dong, J. Modified method for the estimation of groundwater evapotranspiration under very shallow water table conditions based on diurnal water table fluctuations. *J. Hydrol.* **2021**, *597*, 126193. [CrossRef]
24. Wang, T.-Y.; Wang, P.; Yu, J.-J.; Pozdniakov, S.P.; Du, C.-Y.; Zhang, Y.-C. Revisiting the White method for estimating groundwater evapotranspiration: A consideration of sunset and sunrise timings. *Environ. Earth Sci.* **2019**, *78*, 412. [CrossRef]
25. Su, Y.H.; Qi, F.; Zhu, G.F.; Qi, Z. Evaluating the different methods for estimating groundwater evapotranspiration using diurnal water table fluctuations. *J. Hydrol.* **2022**, *607*, 127508. [CrossRef]
26. Nimr, O.A.; Van Putte, N.; Meire, P.; Grygoruk, M.; Verreydt, G.; Grodzka-Łukaszewska, M. Revealing mechanisms regulating diurnal groundwater level fluctuation in a temperate fen peatland: A spatiotemporal exploration. *J. Hydrol.* **2024**, *637*, 131414. [CrossRef]
27. McLaughlin, D.L.; Cohen, M.J. Ecosystem specific yield for estimating evapotranspiration and groundwater exchange from diel surface water variation. *Hydrol. Process.* **2014**, *28*, 1495–1506. [CrossRef]
28. Yue, W.; Wang, T.; Franz, T.E.; Chen, X. Spatiotemporal patterns of water table fluctuations and evapotranspiration induced by riparian vegetation in a semiarid area. *Water Resour. Res.* **2016**, *52*, 1948–1960. [CrossRef]
29. Gumuła-Kawęcka, A.; Jaworska-Szulc, B.; Szymkiewicz, A.; Gorczewska-Langner, W.; Pruszkowska-Caceres, M.; Angulo-Jaramillo, R.; Šimůnek, J. Estimation of groundwater recharge in a shallow sandy aquifer using unsaturated zone modeling and water table fluctuation method. *J. Hydrol.* **2022**, *605*, 127283. [CrossRef]
30. Gribovszki, Z.; Szilágyi, J.; Kalicz, P. Diurnal fluctuations in shallow groundwater levels and streamflow rates and their interpretation—A review. *J. Hydrol.* **2010**, *385*, 371–383. [CrossRef]
31. Wondzell, S.M.; Gooseff, M.N.; McGlynn, B.L. An analysis of alternative conceptual models relating hyporheic exchange flow to diel fluctuations in discharge during baseflow recession. *Hydrol. Process.* **2010**, *24*, 686–694. [CrossRef]
32. McDonald, A.K.; Sheng, Z.; Hart, C.R.; Wilcox, B.P. Studies of a regulated dryland river: Surface-groundwater interactions. *Hydrol. Process.* **2013**, *27*, 1819–1828. [CrossRef]
33. Shah, N.; Nachabe, M.; Ross, M. Extinction depth and evapotranspiration from ground water under selected land covers. *Ground Water* **2007**, *45*, 329–338. [CrossRef] [PubMed]
34. Wang, T.Y.; Yu, J.J.; Wang, P.; Min, L.L.; Pozdniakov, S.P.; Yuan, G.F. Estimating groundwater evapotranspiration by phreatophytes using combined water level and soil moisture observations. *Ecohydrology* **2019**, *12*, e2092. [CrossRef]
35. Xiao, X.; Xu, X.; Huang, G. Analytical expressions of drainable and fillable porosity for layered soils under shallow groundwater environments. *Water Resour. Res.* **2022**, *58*, e2021WR030682. [CrossRef]
36. Tan, S.-C.; Jiang, X.-W.; Zhang, Z.-Y.; Han, P.-F.; Wang, X.-S.; Wan, L.; Zeng, Y.-J. Revisiting the quantitative relationship between groundwater evapotranspiration and water table depth: A numerical study. *J. Hydrol.* **2025**, *658*, 133100. [CrossRef]

37. Lu, Z.; Yang, X. Effects of microtopography on patterns and dynamics of groundwater–surface water interactions. *Adv. Water Resour.* **2024**, *188*, 104704. [CrossRef]
38. Széles, B.; Broer, M.; Parajka, J.; Hogan, P.; Eder, A.; Strauss, P.; Blöschl, G. Separation of scales in transpiration effects on low flows: A spatial analysis in the hydrological open air laboratory. *Water Resour. Res.* **2018**, *54*, 6168–6188. [CrossRef]
39. Harold, R.D. Capillary Properties of Soils—Influence Upon Specific Yield. *Trans. ASAE* **1972**, *15*, 688–0691. [CrossRef]
40. Simunek, J.; Sejna, M.; Van Genuchten, M.T. *The HYDRUS Software Package for Simulating Two- and Three-Dimensional Movement of Water, Heat, and Multiple Solutes in Variably-Saturated Media*; Technical Manual Version 2; PC Progress: Prague, Czech Republic, 2012.
41. Feddes, R.A. Simulation of field water use and crop yield. In *Simulation of Plant Growth and Crop Production*; John Wiley & Sons, Pudoc: Wageningen, The Netherlands, 1982; pp. 194–209.
42. Ritchie, J.T. Model for predicting evaporation from a row crop with incomplete cover. *Water Resour. Res.* **1972**, *8*, 1204–1213. [CrossRef]
43. Shi, J.-X.; Jiang, X.-W.; Zhang, Z.-Y.; Zhang, Y.-P.; Wang, X.-S.; Wan, L. Interaction of focused recharge and deep groundwater discharge near a wetland: A study in the Ordos Basin, China. *J. Hydrol.* **2023**, *626*, 130361. [CrossRef]
44. Zhao, K.Y.; Jiang, X.W.; Wang, X.S.; Wan, L. Restriction of groundwater recharge and evapotranspiration due to a fluctuating water table: A study in the Ordos Plateau, China. *Hydrogeol. J.* **2021**, *29*, 567–577. [CrossRef]
45. Wang, P.; Shang, S.; Rong, Z.; Sun, J.; Ma, J.; Lu, Z.; Wang, F.; Fu, Z. Unraveling belowground community assembly in temperate steppe ecosystems. *Biology* **2025**, *14*, 1350. [CrossRef]
46. Winter, T.C. The concept of hydrologic landscapes. *J. Am. Water Resour. Assoc.* **2001**, *37*, 335–349. [CrossRef]
47. Thompson, C.; Devito, K.J.; Mendoza, C.A. Hydrologic impact of aspen harvesting within the subhumid Boreal Plains of Alberta. *Hydrol. Process.* **2018**, *32*, 3924–3937. [CrossRef]
48. Xie, H.Y.; Jiang, X.W.; Tan, S.C.; Wan, L.; Wang, X.S.; Liang, S.H.; Zeng, Y.J. Interaction of soil water and groundwater during the freezing-thawing cycle: Field observations and numerical modeling. *Hydrol. Earth Syst. Sci.* **2021**, *25*, 4243–4257. [CrossRef]
49. Jiang, X.W.; Sun, Z.C.; Zhao, K.Y.; Shi, F.S.; Wan, L.; Wang, X.S.; Shi, Z.M. A method for simultaneous estimation of groundwater evapotranspiration and inflow rates in the discharge area using seasonal water table fluctuations. *J. Hydrol.* **2017**, *548*, 498–507. [CrossRef]
50. Lee, T.M. Effects of nearshore recharge on groundwater interactions with a lake in mantled karst terrain. *Water Resour. Res.* **2000**, *36*, 2167–2182. [CrossRef]
51. Hokanson, K.J.; Thompson, C.; Devito, K.; Mendoza, C.A. Hummock-scale controls on groundwater recharge rates and the potential for developing local groundwater flow systems in water-limited environments. *J. Hydrol.* **2021**, *603*, 126894. [CrossRef]
52. Winter, T.C. The interaction of lakes with variably saturated porous media. *Water Resour. Res.* **1983**, *19*, 1203–1218. [CrossRef]
53. Zhao, Y.; Liu, Y.; Li, J.; Liu, X. Spatial and temporal variation of potential evapotranspiration and its sensitivity to meteorological factors in China from 1960 to 2013. *Desert Oasis Meteorol.* **2018**, *12*, 1–9. (In Chinese)

Disclaimer/Publisher's Note: The statements, opinions and data contained in all publications are solely those of the individual author(s) and contributor(s) and not of MDPI and/or the editor(s). MDPI and/or the editor(s) disclaim responsibility for any injury to people or property resulting from any ideas, methods, instructions or products referred to in the content.